# Ground and excited states of the NaCl:$Cu^+$ impurity system

Koblar A. Jackson and Chun C. Lin
*Department of Physics, University of Wisconsin, Madison, Wisconsin 53706*
(Received 16 May 1988)

The absorption spectra of transition-metal-doped alkali halide systems are distinguished by characteristic features identified with transitions between electron states localized on the impurity ion. The theoretical description of these features depends on a realistic treatment of the host crystal electronic structure, as well as on the treatment of the impurity ion. The success of recent calculations using the self-interaction-corrected local-spin-density (SIC-LSD) form of density-functional theory in determining the band structure of alkali halide crystals makes SIC-LSD a good candidate for use in the impurity problem. In this work SIC-LSD is applied to the NaCl:$Cu^+$ impurity system, using an embedded-cluster technique explicitly including seven near-neighbor shells of the host crystal ions around the $Cu^+$ site, allowing a full characterization of the low-lying impurity excited states. The calculated values for the fundamental $3d \rightarrow 4s$ and $3d \rightarrow 4p$ impurity-ion transitions are in close agreement with corresponding features of the NaCl:$Cu^+$ absorption spectrum. We compare and contrast our SIC-LSD results with those of other recent calculations for NaCl:$Cu^+$.

## I. INTRODUCTION

In the past 20 or so years, local-density-functional theories[1,2] have become the preeminent tools for the study of large electronic systems. The local-spin-density approximation[3] (LSD) and the Slater statistical exchange approximation[4] ($X\alpha$) have, in particular, been widely used in condensed-matter calculations. The utility of these methods stems from their treatment of the electronic exchange interaction. In Hartree-Fock (HF) theory,[5] treating the exchange interaction exactly results in a gross complication of the single-electron Hamiltonians and the associated self-consistent-field (SCF) equations. The SCF equations are so complicated by exchange terms that HF is very difficult to use without approximation in condensed matter applications.

The local-density theories replace the complicated HF exchange energy with a simpler expression, written as a local functional of the electronic charge density. In the LSD approximation, the precise form of this functional is based on the calculated exchange energy of the uniform electron gas. While use of the approximate exchange energy makes the LSD theory much more convenient to use than HF theory, various problems arise in its application to physical systems. In atomic calculations, for example, atomic total energies and the stability of negative ions are poorly predicted by LSD.[6] In condensed-matter work, it is well known that LSD-based calculations of band gaps in insulators underestimate the experimental band gaps by 30–50%.[7] A more fundamental problem of the theory concerns the physical interpretation of the LSD eigenvalues, i.e., the eigenvalues of the LSD SCF equations. While the eigenvalues of the HF equations may be formally compared to electron ionization energies via Koopmans theorem,[8] no such interpretation is warranted in LSD.

A partial solution to problems arising in LSD is offered by $X\alpha$. In $X\alpha$, an adjustable parameter, $\alpha$, is used to scale the approximate local-density exchange energy. The scaling is done to bring some aspect of the calculated electronic structure into agreement with experiment, or with corresponding HF results. For atoms it is typically the electronic total energy, $E_t^{X\alpha}$, for which such agreement is sought. Calculations have been done[9] to optimize alpha for a large number of atoms to provide agreement between $E_t^{X\alpha}$ and the HF total energy, $E_t^{\mathrm{HF}}$. Calculated ionic crystal band gaps may also be adjusted over a wide range by varying $\alpha$,[10] allowing one to tune $\alpha$ for a given system to match the calculated band gap with experiment. Although it is possible to numerically remedy selected problems of LSD by empirically adjusting $\alpha$, a more fundamental approach to improving LSD is nevertheless desirable.

It has been recognized[6,11] for some time that the exchange approximation used in LSD introduces residual electronic self-interaction energy into the LSD total-energy expression, $E_t^{\mathrm{LSD}}$. The HF total energy customarily includes canceling self-interaction terms in the Coulomb and exchange parts, to give the Coulomb energy and exchange energy separately the full system symmetry; for LSD, however, the cancellation of self-interaction terms is incomplete, since LSD adopts the exact HF Coulomb energy, including the self-interaction terms, while using only an approximate form of the HF exchange energy. The self-interaction correction[6] (SIC) was introduced into LSD to eliminate the residual electronic self-interaction. The SIC-LSD total-energy functional is derived from $E_t^{\mathrm{LSD}}$ by removing exactly the self-Coulomb energy terms, and approximately the self-exchange energy. SCF equations based on the SIC-LSD total-energy functional, $E_t^{\mathrm{SIC-LSD}}$, are self-interaction free, and only slightly more difficult to solve than the corresponding LSD SCF equations. Use of SIC-LSD has proven to effectively address many of the problems associated with LSD. The theory has been successful, for example, in improving the LSD values for atomic total en-

 

ergies, and it correctly predicts the stability of first- and second-row negative ions.[6] Atomic calculations also show that the SIC-LSD eigenvalues are remarkably good approximations of electron ionization energies,[6,12] giving the eigenvalues a compelling physical interpretation similar to that in HF. And in calculations on solids, SIC-LSD yields much improved values for insulator band gaps than are obtained using uncorrected LSD.[7,13]

Transition-metal impurities in ionic crystals have been of interest as prototype impurity systems for many years. Experimentalists have long probed the optical properties of impurity ions in a variety of host crystals.[14,15] Impurity crystal absorption spectra are often characterized by structures due to impurity ion transitions appearing in the otherwise featureless region of the host-crystal spectrum corresponding to the host-crystal band gap. Early theoretical work seeking to understand these impurity features included crystal-field[16] and semiempirical molecular-orbital[17] calculations. In recent years, local-density theories have been applied to these systems to obtain a first-principles description of the impurity electronic structure. The first local-density calculations utilized $X\alpha$: a multiple-scattering $X\alpha$ (MS-$X\alpha$) technique was used for $Cu^+$ and $Ag^+$ impurities in NaCl and later LiCl;[18,19] a separate calculation of the electronic properties of LiCl:$Cu^+$ was made by means of the method of linear combinations of atomic orbitals (LCAO);[10] and a discrete-variation $X\alpha$ (DV-$X\alpha$) method[20] was used for a variety of $Cu^+$ impurity systems. These calculations differ in many respects, for instance, in their treatment of the host-crystal contribution to the impurity Hamiltonian. Each requires, however, the use of a nonuniform exchange parameter, which must be adjusted to meet the needs of both the host-crystal atoms and the impurity ion. HF calculations for $Cu^+$ in NaF and NaCl appeared very recently in the literature.[21,22] Because of the complexity of the exact HF equations, these calculations use a simplified model for the host crystal, and a pseudopotential-like technique to eliminate the host-crystal core states. Finally, the SIC-LSD method has been applied to LiCl:$Cu^+$,[23] in an all-electron LCAO framework. The embedded-cluster approach used in the SIC-LSD work explicitly includes the entire region of the host crystal affected by the introduction of the impurity ion into the host lattice. The results of this calculation for impurity ion transition energies were in very good agreement with experiments, without the use of the empirically adjusted $\alpha$.

In this paper we extend the use of SIC-LSD to the NaCl:$Cu^+$ impurity system. We begin in the next section with an overview of the SIC-LSD theory, exhibiting the SIC-LSD SCF equations, and discussing their general solution. We also discuss the calculation of transition energies in SIC-LSD, and outline a useful computational technique which we later employ in the impurity calculation. We illustrate the use of SIC-LSD by describing its application to the NaCl pure crystal, the free $Cu^+$ ion, and, finally, the NaCl:$Cu^+$ system. The latter calculation adopts the embedded-cluster approach used by Heaton *et al.*[23] for LiCl:$Cu^+$. We briefly highlight the main points of this method, and then take up the particular details of its application to NaCl:$Cu^+$.

In Sec. III we present the results of our NaCl:$Cu^+$ calculation. Discussion of the results follows, where, in addition to comparing with experimental observations, we compare and contrast our results with those of other first-principles calculations on NaCl:$Cu^+$. We end the paper with our conclusions regarding the SIC-LSD calculation, and with our suggestions for future work.

## II. SIC-LSD THEORY

### A. General review

At the heart of the SIC-LSD theory is the SIC-LSD total-energy functional,[6] $E_t^{\mathrm{SIC-LSD}}$. Let us consider an $N$-electron system which is described by the electron density $\rho$, spin density $\rho_\sigma$ ($\sigma=\uparrow$ or $\downarrow$), and orbital densities $\rho_{i\sigma}$. The LSD total energy is

$$E_t^{\mathrm{LSD}}=T+U_{\mathrm{ext}}+\tfrac{1}{2}\int d\mathbf{r}\,d\mathbf{r}'\rho(\mathbf{r})\rho(\mathbf{r}')|\mathbf{r}-\mathbf{r}'|^{-1}-\frac{3}{4}\left[\frac{6}{\pi}\right]^{1/3}\sum_\sigma\int d\mathbf{r}\,\rho_\sigma^{4/3}\,, \tag{1}$$

where $T$ and $U_{\mathrm{ext}}$ are the kinetic energy and external interaction energy (due to the nuclear attraction), respectively, the third term is the Coulomb energy of the $N$ electrons, and the last term is the exchange-correlation energy, written in the Kohn-Sham exchange-only form.[2] The essence of the SIC is to add a term, $U^{\mathrm{SIC}}$, to $E_t^{\mathrm{LSD}}$ in order to remove the exact self-Coulomb interaction, and an approximate form of the self-exchange, i.e.,

$$E_t^{\mathrm{SIC-LSD}}=E_t^{\mathrm{LSD}}+U^{\mathrm{SIC}}\,, \tag{2}$$

$$U^{\mathrm{SIC}}=-\sum_{i,\sigma}\left[\tfrac{1}{2}\int d\mathbf{r}\,d\mathbf{r}'\rho_{i\sigma}(\mathbf{r})\rho_{i\sigma}(\mathbf{r}')|\mathbf{r}-\mathbf{r}'|^{-1}-\frac{3}{4}\left[\frac{6}{\pi}\right]^{1/3}\int d\mathbf{r}\,\rho_{i\sigma}^{4/3}\right]. \tag{3}$$

Here,

$$\rho_{i\sigma}=|\phi_{i\sigma}|^2\,, \tag{4}$$

where $\phi_{i\sigma}$ is a normalized single-electron orbital. We use the Kohn-Sham exchange-only functional for the exchange-correlation energy to illustrate the SIC-LSD theory because of its simple form. Additional correlation functionals may be appended to the Kohn-Sham exchange to account for the effects of electron correlation. The inclusion of correlation terms is straightforward, and will not be discussed further here.

SCF equations for the electronic orbitals are obtained in the standard way by seeking to minimize $E_t^{\mathrm{SIC-LSD}}$ through varying the $\phi$'s. Introducing Lagrange multipliers (LM's), $\lambda_{ij}$, to preserve the orthonormality of the $\phi$'s, we arrive at self-consistent, single-particle Schrödinger-like equations:

$$H_{i\sigma}^{\mathrm{SIC-LSD}}\phi_{i\sigma}=(H_\sigma^{\mathrm{LSD}}+V_{i\sigma}^{\mathrm{SIC}})\phi_{i\sigma}=\sum_j\lambda_{ji}^\sigma\phi_{j\sigma}\,, \tag{5}$$

$$H_\sigma^{\mathrm{LSD}} = -\tfrac{1}{2}\nabla^2 + V_{\mathrm{ext}}(\mathbf{r}) + \int d\mathbf{r}'\rho(\mathbf{r}')|\mathbf{r}-\mathbf{r}'|^{-1} - \left[\frac{6}{\pi}\right]^{1/3}[\rho_\sigma(\mathbf{r})]^{1/3} , \tag{6}$$

$$V_{i\sigma}^{\mathrm{SIC}} = -\int d\mathbf{r}'\rho_{i\sigma}(\mathbf{r}')|\mathbf{r}-\mathbf{r}'|^{-1} + \left[\frac{6}{\pi}\right]^{1/3}[\rho_{i\sigma}(\mathbf{r})]^{1/3} , \tag{7}$$

where $V_{\mathrm{ext}}$ is the "external" potential due to the nuclei. The effective Hamiltonian for the orbital $\phi_{i\sigma}$ is seen to consist of the usual LSD part, $H_\sigma^{\mathrm{LSD}}$, plus a "SIC potential" which, as is evident from Eq. (7), is simply the negative of the Coulomb and exchange self-interaction potentials of the orbital density $\rho_{i\sigma}$.

A distinguishing feature of SIC-LSD theory is the orbital dependence of the total-energy functional, $E_t^{\mathrm{SIC-LSD}}$. This is in contrast to LSD, where $E_t^{\mathrm{LSD}}$ depends only on the total spin densities, $\rho_\sigma$, and not on the individual $\rho_{i\sigma}$. This orbital dependence is inherited by the SIC-LSD SCF equations. More concretely, while $E_t^{\mathrm{LSD}}$ is the same for any set of orthonormal orbitals giving rise to the same spin densities $\rho_\sigma$, $U^{\mathrm{SIC}}$ takes on different values depending on the particular choice of orbitals. Because of the self-Coulomb energy terms, $U^{\mathrm{SIC}}$ is generally more negative for a set of localized $\phi$'s than for a delocalized set. Accordingly, we refer to the set of orbitals corresponding to minimum $E_t^{\mathrm{SIC-LSD}}$ as the local orbitals (LO's). Formal conditions may be generated for the LO's by using the extremum requirement on $E_t^{\mathrm{SIC-LSD}}$ as first outlined by Pederson and Lin.[24] These conditions are called the localization equations (LE's), and are written

$$\langle \phi_{i\sigma}|V_{i\sigma}^{\mathrm{SIC}} - V_{j\sigma}^{\mathrm{SIC}}|\phi_{j\sigma}\rangle = 0 . \tag{8}$$

These equations, which must be satisfied by the exact LO's, have no counterpart in the LSD theory.

The SIC-LSD SCF equations may be expressed in terms of any set of orbitals $\psi$ connected to the LO by a unitary transformation $M$,

$$\phi_{i\sigma} = \sum_\alpha M_{i\alpha}^\sigma \psi_{\alpha\sigma} . \tag{9}$$

If we seek to minimize $E_t^{\mathrm{SIC-LSD}}$ by varying the $\psi$'s and $M$ instead of the $\phi$'s, there results[24]

$$(H_\sigma^{\mathrm{LSD}} + \Delta V_{\alpha\sigma}^{\mathrm{SIC}})\psi_{\alpha\sigma} = \sum_\beta \lambda'^\sigma_{\beta\alpha}\psi_{\beta\sigma} , \tag{10}$$

where

$$\Delta V_{\alpha\sigma}^{\mathrm{SIC}}\psi_{\alpha\sigma} = \sum_i M_{\alpha i}^* V_{i\sigma}^{\mathrm{SIC}}\phi_{i\sigma} , \tag{11}$$

and the additional equations

$$\langle \psi_{\alpha\sigma}|\Delta V_{\alpha\sigma}^{\mathrm{SIC}} - \Delta V_{\beta\sigma}^{\mathrm{SIC}}|\psi_{\beta\sigma}\rangle = 0 . \tag{12}$$

The $\Delta V^{\mathrm{SIC}}$ are the SIC potentials for the $\psi$'s, to be distinguished from the $V^{\mathrm{SIC}}$, which apply to the LO's. Equations (12) are a transformed version of the LE's, satisfied because $M$ is unitary.

It is possible to choose a transformation $M$ that diagonalizes $\lambda'_{\beta\alpha}$ in Eq. (10). The resulting $\psi$'s are the canonical orbitals.[25] The orbital eigenvalue for a given $\psi$ is the removal energy per electron of an infinitesimal amount of orbital charge from that state. It has been shown,[6,12,24] however, that the canonical orbital eigenvalue also well approximates the ionization energy of the corresponding electron. This is an important feature of SIC-LSD not true for uncorrected LSD. In this paper, unless otherwise stated, $\phi$ and $\psi$ denote the LO's and canonical orbitals respectively, or some approximation to them. To solve for $\psi$, it is necessary to have the LO's in order to construct $\Delta V^{\mathrm{SIC}}$ from Eq. (11). Calculating the exact LO's requires a complicated double-iteration procedure;[24] however, since $\Delta V^{\mathrm{SIC}}$ is essentially a correction term, it is possible to obtain accurate $\psi$ using only approximate LO's to construct $\Delta V^{\mathrm{SIC}}$.

The orbital-dependent form of the effective Hamiltonians complicates the solution of the SIC-LSD SCF equations [Eq. (10)]. Of particular concern is maintaining the orthogonality of the $\psi$'s. Many techniques are available to solve such a set of equations, and we elect to transform the set into an eigenvalue equation for a single operator, using a projection-operator technique similar to that found in open-shell Hartree-Fock theory. We write this operator, which we refer to as the unified Hamiltonian,[12] as

$$H_u = \sum_{i=1}^N (P_i H_i P_i + \hat{O}H_i P_i + P_i H_i \hat{O}) , \tag{13}$$

where

$$P_i g(\mathbf{r}) = \psi_i(\mathbf{r})\int d\mathbf{r}'\psi_i^*(\mathbf{r}')g(\mathbf{r}') \tag{14}$$

and

$$\hat{O} = 1 - \sum_{j=1}^N P_j . \tag{15}$$

It is easy to show that the eigenvalue equation for the unified Hamiltonian,

$$H_u\psi_i = \varepsilon_i\psi_i , \tag{16}$$

is equivalent to Eq. (10) at self-consistency, with the $\varepsilon_i$ identified with the diagonal LM, $\lambda'_{ii}$.

The use of SIC-LSD for calculating transition energies has been discussed in the literature.[12,26] For an $N$-electron system, consider a one-electron transition from orbital $a$ to $b$, and write the initial and final electron configurations symbolically as $(N-1)(a)$ and $(N-1)(b)$, respectively. To allow for the orbital relaxation of the $N-1$ passive electrons, the transition energy is taken as the total-energy difference between the two configurations. Using a generalization of the concept of fractional orbital occupancy, it is possible[26] to express this total-energy difference as an integral of the relevant orbital energies, $\varepsilon_a$ and $\varepsilon_b$, along with some correction terms, over $\omega$, an occupation parameter specifying the relative occupation of the ground- and excited-state configurations. This approach avoids directly taking the difference in total energies, which are typically 2 or more

orders of magnitude larger than the transition energies. This method has been used to calculate transition energies for the first- and second-row free atoms,[26] and the $3d \rightarrow 4s$ and $3d \rightarrow 4p$ transition energies for LiCl:$Cu^+$.[23] In addition, an approximate, but much simpler method has been developed[12] for calculating transition energies ($a \rightarrow b$) between localized states. In this method, called the ground-state unoccupied-orbital (GSUO) approximation, one uses the SIC-LSD Hamiltonian for orbital $a$ (the lower state) to calculate the energies (i.e., the eigenvalues of the SIC-LSD SCF equations) of both the occupied orbital $a$ and the unoccupied orbital $b$. Then the transition energy is, to a good approximation, given by the simple difference

$$E_t^{\mathrm{SIC-LSD}}[(N-1)b]-E_t^{\mathrm{SIC-LSD}}[(N-1)a]=\varepsilon_b-\varepsilon_a \ , \tag{17}$$

where

$$\varepsilon_b=\langle \psi_b | H_a^{\mathrm{SIC-LSD}} | \psi_b \rangle \tag{18}$$

and

$$\varepsilon_a=\langle \psi_a | H_a^{\mathrm{SIC-LSD}} | \psi_a \rangle \ . \tag{19}$$

The GSUO scheme has been tested for free atoms and LiCl:$Cu^+$, and gives results close to those obtained by the more rigorous procedure involving the integral over the fractional occupacy, and in close agreement with experiment. The unified Hamiltonian in Eq. (13) applies only to the occupied orbitals. We include the unoccupied excited orbitals by appending an additional term to $H_u$:[12]

$$H_u=\sum_{i=1}^{N}(P_iH_iP_i+\hat{O}H_iP_i+P_iH_i\hat{O})+\hat{O}H_{\mathrm{exc}}\hat{O} \ , \tag{20}$$

where the summation covers the $N$ occupied orbitals, and $H_{\mathrm{exc}}$ is the SIC-LSD Hamiltonian used for the excited orbital, according to the GSUO approximation, the Hamiltonian of the orbital from which the transition originates.

As mentioned above and discussed elsewhere in the literature,[6,12,24] while the SIC-LSD canonical orbital eigenvalue formally corresponds to the removal energy per unit charge of an infinitesimal amount of orbital charge, in practice it is found to be a good approximation to the removal energy of a whole electron. Because of this connection between orbital eigenvalues and ionization energies, it is easy to see that transition energies should be well approximated by the difference between the SIC-LSD orbital eigenvalues as in the GSUO approximation. The GSUO method is adopted in the present work, although we use the more rigorous procedure to check our results (see Sec. III F below).

To study NaCl:$Cu^+$ we start with the electronic structures of the pure NaCl crystal and of the free $Cu^+$ ion. The change in the pure-crystal Hamiltonian, $H_{\mathrm{PC}}$, due to replacing a $Na^+$ ion by $Cu^+$ is introduced and the solution for the impurity crystal is obtained by the LCAO method. The general formalism for this procedure has been presented previously.[23] We will review briefly in the following sections the key points, and those that are relevant to the specific application of the method to NaCl:$Cu^+$.

### B. Electronic structure of the perfect NaCl crystal

Our technique for performing LCAO SIC-LSD calculations for pure alkali halide crystals has been presented in the literature.[7,13] The canonical orbitals for the pure NaCl crystal are the standard Bloch functions. Adding the SIC to the LSD calculation requires identifying a set of LO's in order to obtain $\Delta V^{\mathrm{SIC}}$ in Eqs. (10) and (11). The Wannier functions (WF's), which satisfy Eq. (8), are such a set. Because $\Delta V^{\mathrm{SIC}}$ is a relatively small part of the Hamiltonian, high accuracy in the WF's is not needed. Approximate and computationally simple versions of the WF's have been given in a previous work.[13]

For a simple band, $\psi$ is labeled by the band index $n$ and the crystal momentum $\mathbf{k}$. According to Eq. (11), $\Delta V^{\mathrm{SIC}}$ depends on both $n$ and $\mathbf{k}$. For a narrow band a very good approximation is to assign to the entire band a single potential, $\Delta V_n^{\mathrm{SIC}}$, which is the average of the individual $\Delta V_{n,\mathbf{k}}^{\mathrm{SIC}}$ over $\mathbf{k}$. In the case of a composite band there is a third index labeling the subband, and an averaging over this index, as well as $\mathbf{k}$, is made to obtain $\Delta V_n^{\mathrm{SIC}}$. This averaging process allows us to speak of a single $\Delta V^{\mathrm{SIC}}$ for each band with virtually no loss of accuracy when applied to alkali halides. Heaton and Lin[7] use this averaging to derive a computationally convenient, density-weighted form for the $\Delta V^{\mathrm{SIC}}$. For a $Na^+$ band,

$$\Delta V_n^{\mathrm{SIC}}(\mathbf{r})=\sum_{\nu} V_n^{\mathrm{SIC}}(\mathbf{r}-\mathbf{R}_\nu)\eta_n(\mathbf{r}-\mathbf{R}_\nu)/\rho_n(\mathbf{r}) \ , \tag{21}$$

where the lattice sum covers all the cation sites in the crystal. $V_n^{\mathrm{SIC}}(\mathbf{r}-\mathbf{R}_\nu)$ is the SIC potential based on the local-orbital density, $\eta_n(\mathbf{r}-\mathbf{R}_\nu)$, centered on the site $\mathbf{R}_\nu$. This $\eta_n$ is an approximation of the subband-averaged Wannier density associated with the lattice site, and $\rho_n$ is the total band charge density, the lattice sum of the $\eta_n$. The analogous expression for a $Cl^-$ band $\Delta V^{\mathrm{SIC}}$ sums over the anion sites in the crystal. We use the density-weighted form for $\Delta V^{\mathrm{SIC}}$ [Eq. (21)] in this work. The core states are so localized that the LO's for a core band are identical to the corresponding atomic orbitals, and $\Delta V^{\mathrm{SIC}}$ for a core band within a given unit cell is obtained from $V^{\mathrm{SIC}}$ in Eq. (7) using the appropriate atomic core function. This can readily be seen from Eq. (21) above for $\Delta V^{\mathrm{SIC}}$, given that core densities centered on different lattice sites have virtually no overlap. The effect of SIC on a core band thus amounts to a rigid downward shift in energy. Even for the valence band (VB), the charge overlap between the anions in NaCl is so small that this approximate technique of equating $\Delta V^{\mathrm{SIC}}$ and $V^{\mathrm{SIC}}$ within a given unit cell, although not used in this calculation, is very accurate,[13] providing a simple estimation for the VB $\Delta V^{\mathrm{SIC}}$.

The experimental band gap for NaCl is 8.6 eV.[27] Using LSD alone yields a band gap for NaCl of 4.7 eV. Our SIC-LSD result is 9.6 eV, demonstrating that the inclusion of SIC indeed addresses the LSD band-gap problem. In this calculation the Kohn-Sham exchange-only functional[2] was used. There is evidence that including

correlation in the calculation brings the SIC-LSD result closer to the experimental value.[13] We do not investigate here the use of correlated functionals in the pure-crystal calculation; however, the Kohn-Sham functional gives very good results in calculating atomic transitions,[12,28] and we expect a comparable performance for transitions between the localized impurity states in NaCl:$Cu^+$. The self-consistent NaCl charge density, $\rho_{\mathrm{NaCl}}$, which serves as a reference density in the impurity calculation, is little changed by using correlation in the pure-crystal calculation.

For use in the NaCl:$Cu^+$ calculation, we decompose by curve-fitting $\rho_{\mathrm{NaCl}}$ into a lattice summation of localized densities around the cation sites, $\rho(\mathrm{Na}^+|\mathbf{r})$, and around the anion sites, $\rho(\mathrm{Cl}^-|\mathbf{r})$:

$$\rho_{\mathrm{NaCl}}(\mathbf{r})=\sum_{\nu}[\rho(\mathrm{Na}^+|\mathbf{r}-\mathbf{R}_\nu)+\rho(\mathrm{Cl}^-|\mathbf{r}-\mathbf{R}_\nu-\mathbf{t})]\ , \quad (22)$$

where $\mathbf{R}_\nu$ covers all the cation sites and $\mathbf{t}$ is a vector from a cation site to a nearest-neighbor anion site. Conforming to the ionic character of NaCl, the amount of charge enclosed by $\rho(\mathrm{Na}^+|\mathbf{r})$ and $\rho(\mathrm{Cl}^-|\mathbf{r})$ is constrained to 10 and 18 electrons, respectively.

### C. Electronic structure of the free $Cu^+$ ion

The SIC-LSD calculation for the free $Cu^+$ ion is straightforward. One advantage of the GSUO approximation is that we obtain the $3d$, $4s$, and $4p$ orbital energies with only one SCF calculation. The calculated $3d\rightarrow 4s$ and $3d\rightarrow 4p$ transition energies are, respectively, 3.21 and 9.21 eV, which compare well with the experimental values of 3.03 and 8.81 eV.[29] These results are compiled in Table I for later reference.

### D. Electronic structure of NaCl:$Cu^+$

Our first step is to construct the LSD Hamiltonian for the impurity crystal system. We reference the impurity crystal electron density to that of the pure crystal as

$$\rho_{\mathrm{IC}}=\rho_{\mathrm{PC}}+\delta\rho\ , \quad (23)$$

where the subscripts IC and PC refer to the impurity- and pure-crystal systems, respectively. The corresponding increment to the LSD potential consists of a nuclear term arising from the difference in nuclear charge, $\Delta Z$, between Cu and Na, a Coulomb term, and an exchange term:

$$H_{\mathrm{IC}}^{\mathrm{LSD}}=H_{\mathrm{PC}}^{\mathrm{LSD}}+\delta V^{\mathrm{LSD}}\ , \quad (24)$$

$$\delta V^{\mathrm{LSD}}=-\frac{\Delta Z}{r}+\int d\mathbf{r}'\delta\rho(\mathbf{r}')|\mathbf{r}-\mathbf{r}'|^{-1}-\left[\frac{6}{\pi}\right]^{1/3}\{[\rho_{\mathrm{IC}}(\mathbf{r})]^{1/3}-[\rho_{\mathrm{PC}}(\mathbf{r})]^{1/3}\}\ . \quad (25)$$

Since the $Cu^+$ ion is known to be an on-site substitution in the NaCl lattice,[19] the above expressions reflect our choice of the impurity site as the origin of coordinates for the calculation. In this paper we neglect the possible lattice relaxation of the ions neighboring the impurity. This point will be discussed in Sec. III E. An initial approximation to $\delta\rho$ is the difference between the electron density of the free $Cu^+$ ion and $\rho(\mathrm{Na}^+|\mathbf{r})$ defined in Eq. (22). We calculate $\delta V^{\mathrm{LSD}}$ from Eq. (25) on a mesh of points around the impurity site and fit it to $-(\Delta Z/r)e^{-\gamma r^2}$ plus a number of $e^{-\omega r^2}$ Gaussians. Since our basis functions are also in Gaussian form (see below), the matrix elements of $\delta V^{\mathrm{LSD}}$ reduce to multicenter Gaussian integrals, which can be evaluated analytically. $H_{\mathrm{PC}}^{\mathrm{LSD}}$ has already been obtained in terms of Gaussian functions in our pure-crystal calculation, and its matrix elements for the impurity crystal are readily evaluated.

Determination of $\Delta V^{\mathrm{SIC}}$ requires identifying a set of LO's for the impurity crystal. In the case of a pure crystal the LO's are the WF's, which are well approximated by modified forms of the atomic orbitals. With a point defect in the crystal, the LO's are the generalized WF's (GWF's),[23,30] which are site dependent because of the loss of translational symmetry. The GWF's for the point-defect system approach the perfect-crystal WF's exponentially with increasing distance from the defect site.[30] The GWF's for NaCl:$Cu^+$ near the $Cu^+$ site are expected to be atomiclike, but rigorous calculations are very difficult. In Ref. 23 a method for obtaining approximate LO densities is given. (The computational procedure is straightforward, but the equations describing the procedure are lengthy and will not be reproduced here.) From the approximate LO densities at each site the corresponding $V^{\mathrm{SIC}}$ is calculated from Eq. (7) and inserted in Eq. (21) to find the band-averaged $\Delta V^{\mathrm{SIC}}$. For this purpose each of the $1s,2s,\ldots,3d$ manifolds of the $Cu^+$ levels is considered a separate band.

The impurity-crystal wave functions are expanded in a basis set that includes atomic orbitals for the occupied states of the impurity ion and the host-crystal ions out to the seventh-nearest-neighbor shell [(220) in units of the Na-Cl near-neighbor distance, $d_{\mathrm{Na\text{-}Cl}}$]. In addition, we include atomic $Cu^+$ $4s$ and $4p$ orbitals on the defect site. To further strengthen the variational freedom, we supplement the basis functions by single Gaussian orbitals (SGO's) of exponents: $\beta_1=2.608\,63$, $\beta_2=1.829\,02$, $\beta_3=1.2849$, $\beta_4=0.997\,212$, $\beta_5=0.950\,083$, $\beta_6=0.448\,205$, $\beta_7=0.444\,62$, $\beta_8=0.430\,941$, $\beta_9=0.189\,272$, $\beta_{10}=0.140\,12$, $\beta_{11}=0.096$, and $\beta_{12}=0.050\,791$. These SGO's are distributed on the various sites in the following way. Four $s$-type ($\beta_4,\beta_7,\beta_{10},\beta_{12}$), four $p$-type ($\beta_1,\beta_4,\beta_7,\beta_{10}$), and three $d$-type ($\beta_4,\beta_7,\beta_{10}$) SGO's are placed at the defect site. We use four $s$-type and four $p$-type SGO's ($\beta_5,\beta_6,\beta_9,\beta_{11}$) to augment the atomic orbitals on the nearest-neighbor $Cl^-$ shell, and add three $s$-type and three $p$-type SGO's ($\beta_5,\beta_6,\beta_9$) to the next $Cl^-$ shell. Finally, for the nearest $Na^+$ shell, three $s$-type and three $p$-type SGO's ($\beta_2,\beta_3,\beta_9$) are appended.

The cluster basis described here, with significant variational freedom near the impurity site and minimal atomic basis sets "cushioning" the outer edge of the cluster, is used to properly embed the impurity cluster in the bulk crystal. The use of such a basis has been shown[31] to minimize surface effects which arise from representing the states of an infinitely extended Hamiltonian [see Eq. (24)]

with a finite basis.

With the initial approximation for $\delta V^{\mathrm{LSD}}$ and the LO's, we construct the zeroth-order Hamiltonian, which includes $[H_{\mathrm{PC}}^{\mathrm{LSD}}]^{(0)}$, $[\delta V^{\mathrm{LSD}}]^{(0)}$, and $[\Delta V^{\mathrm{SIC}}]^{(0)}$ as a summation of Gaussian-type functions centered on different lattice sites. With the basis functions expressed in terms of Gaussian orbitals, the Hamiltonian and overlap matrix elements are evaluated analytically. Solving the LCAO secular equation gives rise to the first-iteration electron density, $\rho_{\mathrm{IC}}^{(1)}$, and hence $\delta\rho^{(1)}$ [see Eq. (23)]. $\delta\rho^{(1)}$ is of very short range, and can be accurately fitted to a superposition of exponential-type functions centered at the $Cu^+$ site and at the first-nearest-neighbor–shell sites. The second term in Eq. (25) can then be integrated analytically, yielding a mesh of numerical values of $[\delta V^{\mathrm{LSD}}]^{(1)}$, which is fitted to a mixture of Gaussian-type functions centered at the $Cu^+$ site and the six surrounding $Cl^-$ sites. Likewise, from the first-iteration eigenfunctions we determine a set of first-iteration LO's, which yield $[\Delta V^{\mathrm{SIC}}]^{(1)}$ through the use of Eqs. (7) and (21). The iteration cycle continues until self-consistency is reached.

## III. RESULTS AND DISCUSSION

### A. Energy levels and transition energies

The ground state of the free $Cu^+$ ion has the closed-shell configuration $1s^2 2s^2 2p^6 3s^2 3p^6 3d^{10}$. In the impurity system the crystal field breaks the degeneracy of the free-ion $d$ orbitals into doubly- and triply-degenerate states corresponding to the $E_g$ and $T_{2g}$ representations of the $O_h$ group, the $T_{2g}$ states lying at lower energy in the crystal field. In our NaCl:$Cu^+$ calculation, eigenstates corresponding to the occupied $Cu^+$ free-ion states are highly localized on the $Cu^+$ site, so that, for example, it is meaningful to speak of $Cu^+$ $3d$ states in the impurity crystal. Eigenstates corresponding to the $Cu^+$ $4s$ and $4p$ free-ion orbitals are somewhat less localized on the defect site (see the discussion below), but we shall nonetheless refer to them as impurity $Cu^+$ $4s$ and $4p$ states for simplicity. In this work, we are concerned with the energy of transitions between the $Cu^+$ $3d$ and $Cu^+$ $4s$ and $4p$ impurity states, i.e., $3de_g, 3dt_{2g} \rightarrow 4s$, and $3de_g, 3dt_{2g} \rightarrow 4p$. Although the $3d \rightarrow 4s$ transitions are dipole forbidden in the free ion, they are made partially allowed in the impurity crystal through vibronic coupling to odd-parity phonon modes.

Figure 1 is a portion of the eigenvalue spectrum obtained in our fully-self-consistent calculation of the NaCl:$Cu^+$ electronic structure. Using the LCAO eigenvectors, the atomic-orbital parentage of the eigenstates is easily traced, allowing clear identification of states associated with the $Cu^+$ ion. The positions of the $Cu^+$ $3d$, $4s$, and $4p$ eigenvalues are shown explicitly in Fig. 1. The positions of the impurity-crystal valence-band (VB) states are also shown, with the pure-crystal VB and conduction-band (CB) boundaries shown for reference.

The calculated $3de_g \rightarrow 4s$ and $3dt_{2g} \rightarrow 4s$ transition energies are 4.77 and 5.28 eV, respectively, in good agreement with the corresponding experimental values[20] of 4.36 and 4.77 eV. For the $3de_g \rightarrow 4p$ and $3dt_{2g} \rightarrow 4p$ transitions, our calculated values are 8.21 and 8.72 eV, respectively. Experimentally, a broad peak (2.5 eV wide) at 7.29 eV was attributed to the $3d \rightarrow 4p$ absorption.[32] The poorer agreement between theory and experiment here may be partly due to the uncertainty in determining the experimental value for the transition energy because of the very large width of the observed absorption signal. In Table I we summarize the calculated and observed values of the $3d \rightarrow 4s$ and $3d \rightarrow 4p$ transitions.

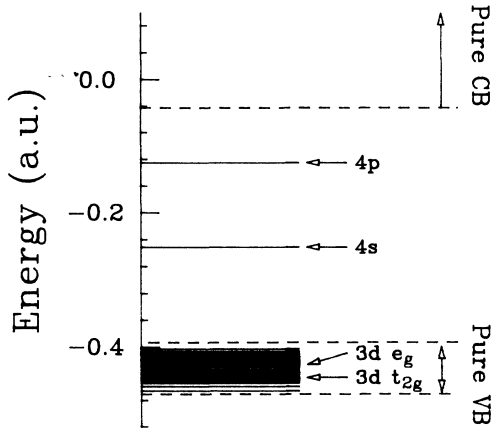


FIG. 1. Calculated energy levels of the $3d$, $4s$, and $4p$ impurity states and the host-crystal valence-band states of NaCl:$Cu^+$. The ranges of the valence bands and conduction bands of the pure crystal are indicated.

### B. The nature of the impurity states

Table I exhibits a characteristic feature of all NaCl:$Cu^+$-type impurity systems: the increase in the $3d \rightarrow 4s$ transition energy in the impurity crystal over the corresponding free-ion transition. This general feature has been previously explained[33,10] by an argument concerning the mixing of the $Cu^+$ $3d$ and $4s$ orbitals with the $3p$ orbitals centered on the nearest-neighbor, or ligand, $Cl^-$ ions to form bonding-antibonding pairs of impurity eigenstates. The energy of the bonding partner in such a pair is lowered as a result of the mixing, and that of the antibonding partner is raised. Because the $Cu^+$ $4s$ orbital is more diffuse and has greater overlap with the ligand orbitals, the effect of this bonding-antibonding is more pronounced for the $Cu^+$ $4s$ than for the $Cu^+$ $3d$ states, and the antibonding $Cu^+$ $4s$ eigenvalue is therefore raised by the interaction with the ligand orbitals relative to the $3d$ eigenvalues, resulting in the observed increase in the $3d \rightarrow 4s$ energy. In this argument, the $Cu^+$ $3d$ states are

TABLE I. Theoretical and experimental values of the $3d \rightarrow 4s$ and $3d \rightarrow 4p$ transition energies (in eV) for a free $Cu^+$ ion and for NaCl:$Cu^+$.

| | Free $Cu^+$ | | NaCl:$Cu^+$ | |
|---|---|---|---|---|
| Transitions | Theor. | Expt. | Theor. | Expt. |
| $3de_g \rightarrow 4s$ | 3.21 | 3.03 | 4.77 | 4.36 |
| $3dt_{2g} \rightarrow 4s$ | 3.21 | 3.03 | 5.28 | 4.77 |
| $3de_g \rightarrow 4p$ | 9.21 | 8.81 | 8.21 | 7.29 |

assumed to be antibonding, but, as we discuss in subsection D below, this depends on the specific system being considered. We note here that the general argument predicts an increase in the $3d \rightarrow 4s$ energy whether or not the $Cu^+$ $3d$ states are distinctly antibonding, so long as the $Cu^+$ $4s$ remains more strongly antibonding than the $Cu^+$ $3d$ state. The SIC-LSD results for NaCl:$Cu^+$ support the general explanation for the shift in the impurity transition energy. We show this by considering in this section the nature of the $Cu^+$ $3d$ and $4s$ impurity states, demonstrating that the $Cu^+$ $4s$ state is less localized and has a larger admixture of ligand orbitals than the $Cu^+$ $3d$ states. To determine the degree to which the $Cu^+$ orbitals mix with the ligand orbitals in the impurity eigenstates, we performed a Mulliken population analysis[34] on the self-consistent eigenfunctions. The population analysis gives the distribution by ion shell of the charge associated with each of the eigenstates. The $Cu^+$ $3d$ states are well localized on the impurity site, with 95% and 99% of the electron charge associated with the $Cu^+$ ion for the $3de_g$ and $3dt_{2g}$ states, respectively, reflecting the small mixing of the ligand $3p$ orbitals into these states.

The $Cu^+$ $4s$ and $4p$ orbitals are more diffuse than the $3d$ orbitals, and undergo heavier mixing with the ligand orbitals in the impurity eigenstates. The standard Mulliken analysis breaks down for these states, because of the large overlap of the long-range SGO's contributing heavily to the respective eigenfunctions. We may investigate the nature of these states using an alternative method,[10] however, by systematically monitoring the dependence of the computed $4s$ and $4p$ eigenvalues on the presence of various SGO's in the fixed-basis set. The nature of the fixed basis is such that the occupied eigenstates of the impurity system are represented almost entirely by the corresponding atomic orbitals in the basis, while the unoccupied eigenstates are represented by the $Cu^+$ $4s$ and $4p$ atomic orbitals and the various SGO's. (This reflects the fact that the atomic orbitals are good approximations of the LO's for this system.) Removing SGO's reduces the variational freedom of the basis, greatly degrading the representation of the unoccupied states. As a result, the eigenvalues for these states become less negative. By establishing the sensitivity of the $4s$ and $4p$ eigenvalues to the presence of SGO's centered on specific shells, we therefore indirectly determine the spatial extent of the eigenfunctions. Starting with the full basis set as listed in Sec. II D, called set (a), we first remove all the SGO's in the third-nearest-neighbor shell to form set (b). Removal of the SGO's in the second- and third-nearest-neighbor shells generates set (c). Set (d) contains SGO's only on the impurity site, i.e., none on any of the host-crystal sites, and set (e) is the minimal set with all SGO's removed. The $Cu^+$ $4s$ eigenvalues for basis sets (a)–(e) are $-0.2647$, $-0.2646$, $-0.2645$, $-0.2624$, and $-0.2545$ a.u., respectively. The $4s$ energy level is seen to depend most on the SGO's from the $Cu^+$ site; the ligand-shell SGO's are seen to be less important, and the SGO's on the second- and third-near-neighbor shells have almost no effect on the eigenvalue. From this we see that the impurity $Cu^+$ $4s$ state is well localized on the $Cu^+$ site and the ligand shell. The importance of the $Cu^+$ SGO's indicates the distortion of the impurity $4s$ state in the region around the $Cu^+$ ion due to the interaction with the ligands. (For comparison, the $Cu^+$ $3d$ energy level is virtually unchanged upon removing all SGO's from the basis.) With the strongly overlapping SGO's removed from the basis, the Mulliken analysis shows 85% of the $4s$ charge centered on the $Cu^+$ ion, and 15% on the ligand shell. While these numbers do not provide a detailed charge distribution for the true $4s$ state, they are an added indication that the $4s$ state has a larger admixture of ligand orbitals than the more localized $3d$ states. For the $4p$ eigenvalues the five basis sets (a)–(e) give $-0.1319$, $-0.1312$, $-0.1310$, $-0.1182$, and $-0.0956$ a.u., respectively. Here the SGO's on the nearest neighbors are indispensable, and even the SGO's on the second nearest neighbors ($Na^+$) have an appreciable influence. In the pure-crystal calculation, the SGO's represent conduction-like states. The importance of SGO's centered on the ligand shell and the $Na^+$ shell suggests that the $4p$ state has some CB character. The decrease in the $3d \rightarrow 4p$ transition energy in the impurity compared with the free ion is the result of the mixing of the $Cu^+$ $4p$ orbital with CB states. This mixing produces an impurity state extending over the first few ion shells around the defect site; through the mixing, the eigenvalue of this impurity $4p$ state is lowered relative to the $Cu^+$ $3d$ eigenvalues.

### C. Comparison with other NaCl:$Cu^+$ calculations

Many calculational schemes have been applied to NaCl:$Cu^+$-type impurity systems. In the past few years, three separate calculations specifically treating NaCl:$Cu^+$ have been presented in the literature, two[19,20] using $X\alpha$-based methods, and the other a LCAO Hartree-Fock (HF) formalism.[22] To aid in the comparison of the various results, it is appropriate to first discuss a few points concerning each of these calculations. Chermette and Pedrini[19] use a multiple-scattering $X\alpha$ (MS-$X\alpha$) cluster method in their calculation of NaCl:$Cu^+$. MS $X\alpha$ is a muffin-tin-based formalism: the $X\alpha$ potential seen by the electrons is assumed spherically symmetric inside muffin-tin spheres centered on the impurity crystal ion sites, and constant in the region between the spheres. The exchange parameter $\alpha$ takes on different values in the muffin-tin spheres for each of the different ion types in NaCl:$Cu^+$. The cluster method used in the work of Chermette and Pedrini explicitly treats only the central $Cu^+$ impurity ion and the six surrounding ligand ions; the remainder of the host crystal is modeled by a $9 \times 9 \times 9$ array of uniformly charged spheres centered on the crystal lattice sites around the $CuCl_6$ cluster. The host-crystal contribution to the impurity potential is taken to be the classical electrostatic potential due to the charged spheres. The $X\alpha$ SCF equations are solved using standard multiple-scattering techniques, and transition energies are calculated using Slater's transition-states method.

The discrete-variation $X\alpha$ (DV-$X\alpha$) treatment of Payne, Goldberg, and McClure[20] for NaCl:$Cu^+$ shares many of the features of the MS-$X\alpha$ method, including the

simple model for the host-crystal contribution to the impurity potential and the transition-states method for calculating transition energies. The DV-$X\alpha$ method, however, employs a different computational procedure for solving the SCF equations.

As in the two $X\alpha$ calculations, only the $Cu^+$ and the six ligand ions are treated explicitly in the HF calculation of Winter, Pitzer, and Temple.[22] In fact, only the valence electrons on the $Cl^-$ ions are included: the core orbitals are removed from the calculation via a pseudopotential-like technique. The $Cl^-$ $3p$ orbitals appearing in the basis set are pseudo-wave-functions which coincide with real $3p$ functions in regions outside the range of the $Cl^-$ core electrons, but which are smooth inside the core region, lacking the orthogonality spikes of true atomiclike $3p$ orbitals. The host crystal in this calculation is modeled by an array of point ions and total ion potentials (again similar to pseudopotentials) centered on 125 lattice sites around the impurity ion. Transition energies are calculated directly by taking the difference in HF total energies of the ground and excited states.

In Table II transition energies for the $Cu^+$ $3d \rightarrow 4s$ transitions are compared. The GSUO approximation used to obtain the transition energies in our SIC-LSD calculation is effectively spin polarized, with the active electron assigned the same spin in the ground and excited configurations. Our transition energies therefore represent an average of the transitions to the spin-singlet ($S=0$) and -triplet ($S=1$) excited states.[35] In the HF and MS-$X\alpha$ calculations, the singlet and triplet transitions were considered separately. In order to compare with the SIC-LSD results, the average of the singlet and triplet transition energies found in these calculations is shown in Table II. The DV-$X\alpha$ calculation reports only the average of the $3de_g$ and $3dt_{2g} \rightarrow 4s$ transitions; this average is the value appearing in the table. The bottom row in Table II is the energy difference between the transitions originating from the $3de_g$ and $3dt_{2g}$ states, respectively, i.e., the spacing between the two main peaks (the $E_g$ and $T_{2g}$ peaks) in the NaCl:$Cu^+$ absorption spectrum. (For HF and MS-$X\alpha$, this difference is calculated using the spin-multiplet-averaged values for the $E_g$ and $T_{2g}$ transitions appearing in the table; virtually the same value is found by taking the difference between the singlet or triplet transitions individually.)

TABLE II. Comparison of the $3d \rightarrow 4s$ transition energies (in eV) calculated by different methods. The energy spacings between the $3de_g \rightarrow 4s$ and $3dt_{2g} \rightarrow 4s$ transitions, denoted $\Delta$, are included.

| LSD[a] | SIC[a] | HF[b] | DV-$X\alpha$[a] | MS-$X\alpha$[c] | MS-$X\alpha$[d] |
|---|---|---|---|---|---|
| $3de_g \rightarrow 4s$ | 4.77 | 3.08 | 3.35[e] | 4.26 | 3.74 |
| $3dt_{2g} \rightarrow 4s$ | 5.28 | 3.23 | | 5.25 | 4.31 |
| $\Delta$ | 0.51 | 0.15 | 0.41 | 0.99 | 0.57 |

[a]GSUO approximation.
[b]Average of the singlet and triplet transition energies (see text).
[c]Average of the singlet and triplet transition energies (see text). Cu-Cl distance 5.31 a.u.
[d]Average of the singlet and triplet transition energies (see text). Cu-Cl distance 5.79 a.u.
[e]Average of the $3de_g \rightarrow 4s$ and $3dt_{2g} \rightarrow 4s$ transition energies.

In Table II is shown the range of $3d \rightarrow 4s$ transition energies predicted by the various calculations. While the SIC-LSD results slightly overestimate the observed transition energies, the other calculations underestimate experiment to varying degrees. The largest deviation from experiment is seen in the HF results, where the calculated transition energies undercut experiment by about 1.3 eV. This underestimate is attributed by Winter *et al.*[22] to the neglect of electron correlation in the HF treatment. They show that the corresponding free-ion transition energies are also underestimated by HF, by 1.52 eV. Since the discrepancy in the free-ion transition energy relative to experiment is attributed to electron correlation, it is reasonable to expect the neglect of correlation to produce a similar problem in the impurity-crystal calculation. The HF calculation also underestimates the energy spacing between the $E_g$ and $T_{2g}$ peaks in the absorption spectrum. This, too, may be due to the neglect of correlation. Winter *et al.*[22] cite a calculation by Shaskin and Goddard[36] on a $Cu^{2+}$ impurity in a fluoride crystal in which configuration interaction (CI) is used to account for electron correlation. The use of CI in that work increased the spacing between the $E_g$ and $T_{2g}$ peaks, leading to better agreement with experiment. No attempt to use CI in the NaCl:$Cu^+$ calculation was made.

The $3d \rightarrow 4s$ transition energies determined in the two $X\alpha$ studies are also significantly smaller than the SIC-LSD results. The MS-$X\alpha$ results[19] are closer to both experiment and SIC-LSD than those of DV-$X\alpha$. The MS-$X\alpha$ calculation was done using a series of values for the Cu-Cl spacing, $d_{\text{Cu-Cl}}$, in order to determine the equilibrium spacing (see the discussion below of lattice relaxation). Chermette and Pedrini[19] found the transition energies to be sensitive to the Cu-Cl distance, decreasing with increasing $d_{\text{Cu-Cl}}$. The authors determined the transition energies over a range of $d_{\text{Cu-Cl}}$ values. The transition energies given in the last column of Table II were obtained for their equilibrium value for $d_{\text{Cu-Cl}}$, 5.79 a.u., which is much larger than the Na-Cl distance in the host crystal, $d_{\text{Na-Cl}}$, 5.33 a.u. In the fourth column of Table II are the MS-$X\alpha$ results for a spacing of 5.31 a.u. Using this value for $d_{\text{Cu-Cl}}$, they calculate 4.26 and 5.25 eV, respectively, for the $3de_g \rightarrow 4s$ and $3dt_{2g} \rightarrow 4s$ transitions, in reasonable agreement with our results and with experiment. (In our calculation, we set $d_{\text{Cu-Cl}}$ equal to $d_{\text{Na-Cl}}$.) The DV-$X\alpha$ transition energy,[20] calculated with $d_{\text{Cu-Cl}}$ equal to $d_{\text{Na-Cl}}$, is much smaller than those of either SIC-LSD or MS-$X\alpha$. We are unable to explain the discrepancy between the DV-$X\alpha$ calculation and the MS-$X\alpha$ calculation for $d_{\text{Cu-Cl}}=5.31$ a.u. The transition-state formalism is used in both calculations to determine the transition energies.

We note that energies for the $3d \rightarrow 4p$ transitions were computed only in the SIC-LSD calculation. This reflects an advantage of our embedded-cluster technique over the other methods in including a number of host-crystal shells around the defect site. Because we include a significant portion of the impurity crystal explicitly in the calculation, we are able to represent the $Cu^+$ $4p$ state and investigate its mixing with conductionlike states. By contrast, the single-shell models for the host crystal used in

the HF and $X\alpha$ calculations are inappropriate for treating the rather more extended $Cu^+$ $4p$ impurity state.

As the transition-energy comparisons in Table II are limited to the $3d \rightarrow 4s$ transitions, discussion of the electron-population results from the different calculations must be limited to the $Cu^+$ $3d$ impurity states, since only these states are comparably represented in all four calculations. Because we include VB orbitals on three near-neighbor $Cl^-$ shells, whereas the other calculations include only ligand-shell VB orbitals, the VB states in our SIC-LSD calculation have a much different character than those in the other works, making a detailed quantitative comparison of population results for those states meaningless. For the $Cu^+$ $3d$ eigenstates, all the calculations show the $3d$ charge density predominantly localized on the impurity ion, with a much smaller amount of charge attributed to the ligand shell. The MS-$X\alpha$ calculation[19] allots 93% of the $3de_g$ charge and 97% of the $3dt_{2g}$ charge to $Cu^+$, whereas the corresponding charge apportionment is 86% and 98% in the DV-$X\alpha$ study.[20] Both $X\alpha$ calculations are in good agreement with the SIC-LSD results of 94% and 99%. In each of the local-density calculations, the $E_g$ state has more charge attributed to the ligand shell than does the $T_{2g}$ state, indicating a greater mixing of $Cu^+$ and ligand orbitals in the $Cu^+$ $3de_g$ eigenfunctions. This is in accord with the geometrical fact that the $3de_g$ orbitals have greater overlap with the ligand $3p$ orbitals than do the $3dt_{2g}$ orbitals. In contrast to these results, the HF calculation[22] shows the $T_{2g}$ state to have the larger ligand-shell charge component. Also, the HF results show a much greater delocalization of the $Cu^+$ $3d$ charge generally than seen in the other calculations. Only 78% and 75% of the charge is attributed to the $Cu^+$ site, respectively, for the $3de_g$ and $3dt_{2g}$ states. The enhanced mixing of $Cu^+$ and $Cl^-$ orbitals in the $T_{2g}$ state in this calculation may result from a near degeneracy of the $Cu^+$ $3dt_{2g}$ and the ligand $Cl^-$ $3p$ orbitals; such a degeneracy would lead to strong mixing of the orbitals in the eigenfunctions. Since the $3de_g$ orbitals lie at higher energy than the $3dt_{2g}$ orbitals, near degeneracy with the $Cl^-$ $3p$ orbitals would not contribute as much to the mixing in the $E_g$ states. One may speculate that the use of the pseudopotential-like technique in the HF calculation may be partly responsible for the increased delocalization of both the $Cu^+$ $3d$ states over the other calculations. In the SIC-LSD calculation, for example, the impurity states arising from the mixing of the $Cu^+$ $3d$ and ligand $3p$ orbitals are constrained to be orthogonal to the $Cu^+$ and $Cl^-$ core states. In the HF calculation, the $Cl^-$ core states do not appear explicitly in the basis, so that the orthogonality constraint is not directly enforced through the SCF process. This may lead to greater mixing of the orbitals as a way to concentrate charge near the $Cl^-$ nuclei, thereby lowering the total energy.

### D. The impurity density of states

Figure 2 is a density-of-states (DOS) plot for the SIC-LSD impurity eigenstates lying in the energy range spanned by the pure-crystal VB, obtained by a 0.1-eV Gaussian broadening of the discrete impurity-crystal eigenvalues. For comparison, a similar plot for states obtained from the pure-crystal Hamiltonian is also shown. The similarity of the two plots is striking. The most significant difference between the two is the slight bump appearing at the bottom of the impurity VB and not present in the pure-crystal plot. The $X\alpha$ work of Harrison and Lin[10] on LiCl:$Cu^+$ provides a qualitative guide to interpreting the NaCl:$Cu^+$ DOS. In that study, a number of small bumps appeared just below the pure-crystal VB in the impurity DOS. These features were identified with the bonding partners of the $Cu^+$ $3d$ and $Cu^+$ $4s$ impurity states, the energies of these states sufficiently lowered through bonding that they were split off below the bulk of the VB. The single extra feature in the NaCl:$Cu^+$ impurity DOS can likewise be identified (using the LCAO eigenvectors) with the bonding partner of the $Cu^+$ $4s$ state; however, no evidence of bonding partners for the $Cu^+$ $3d$ states can be found below the VB in Fig. 2. The absence of extra features in the NaCl:$Cu^+$ DOS may be explained by considering the relative positions of the $Cu^+$ $3d$ and the VB states in the eigenvalue spectrum. As seen in Fig. 1, the $Cu^+$ $3d$ states lie in the middle of the impurity VB. Analysis of the LCAO eigenfunctions for the relevant VB states shows that the $Cu^+$ $3d$ orbitals contribute to states both above and below the impurity $3d$ levels in energy, so that the $3d$ states have neither clearcut bonding nor antibonding character. Accordingly, the $Cu^+$ $3d$ orbitals are only weakly admixed into any given VB state. By contrast, the $Cu^+$ $4s$ state is clearly antibonding, and its bonding partner is readily identified in the impurity DOS. The charge associated with this state is well localized on the $Cu^+$ ion and ligand shell (8% and 72%, respectively) as a result of the bonding. The fact that the $Cu^+$ $3d$ states are not clearly anti-

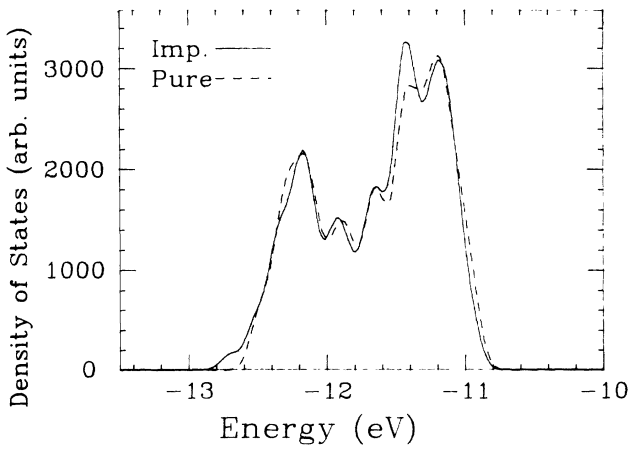


FIG. 2. Density of states of the valence bands of the pure NaCl crystal (dashed curve) and of NaCl:$Cu^+$ (solid curve). The small structure in the solid curve below −12.7 eV is associated with impurity-related states (see Sec. III D).

bonding in NaCl:$Cu^+$ does not affect the explanation for the increase in the $3d \rightarrow 4s$ transition in the impurity: As mentioned above, the $4s$ state must simply be more antibonding than the $3d$ states for the transition energy to increase. Clearly this condition is satisfied for NaCl:$Cu^+$, where the $Cu^+$ $3d$ states are neutrally bonded. Indeed, as the lattice constant increases in the series LiCl:$Cu^+ \rightarrow$NaCl:$Cu^+ \rightarrow$KCl:$Cu^+$, the change in the Madelung shift of the various energy levels (due to the electrostatic interaction with the net $+e$ and $-e$ charges on the ion sites) will move the $Cu^+$ $3d$ levels from a position above the VB to a position below the VB. The character of the impurity $3d$ states can thus be expected to change from antibonding to neutral to bonding in this series. At the same time, the $Cu^+$ $4s$ level remains well above the VB in all three systems, so that the $Cu^+$ $4s$ state remains antibonding in each. The net effect of bonding-antibonding in all three cases is therefore an increase in the impurity $Cu^+$ $3d \rightarrow 4s$ energy over the free ion, and such an increase is seen experimentally for each system.[15,20]

### E. Lattice relaxation

The equilibrium distance between the $Cu^+$ ion and the near-neighbor $Cl^-$ ions, $d_{\text{Cu-Cl}}$, in NaCl:$Cu^+$ remains an open question at the present time. The close comparison of the $Na^+$ and $Cu^+$ ionic radii, 1.85 and 1.81 a.u., respectively (0.98 and 0.96 Å), suggests $d_{\text{Cu-Cl}}$ should be very close to the near-neighbor spacing in NaCl, $d_{\text{Na-Cl}}$, 5.33 a.u. (2.82 Å). Calculations predicting $d_{\text{Cu-Cl}}$ have not, however, yielded consistent results. The HF (Ref. 2) and MS-$X\alpha$ (Ref. 19) calculations discussed above both seek to determine the equilibrium Cu-Cl spacing by systematically computing the total energy of the impurity system for a range of $d_{\text{Cu-Cl}}$ values. The HF calculation predicts $d_{\text{Cu-Cl}}$ to be nearly equal to $d_{\text{Na-Cl}}$, while the MS-$X\alpha$ calculation predicts a substantial outward relaxation of the $Cl^-$ ions in the impurity (5.79 versus 5.33 a.u.). Considering the near equality of the free-ion radii for $Na^+$ and $Cu^+$, the HF result is intuitively reasonable, whereas a significant outward relaxation of the ligands is quite unexpected. Because of the discrepancy in the existing theoretical values of $d_{\text{Cu-Cl}}$, and because we are presently unable to determine an equilibrium value for $d_{\text{Cu-Cl}}$ in the SIC-LSD calculation, we choose instead to rely on the near equality of the $Na^+$ and $Cu^+$ radii and set $d_{\text{Cu-Cl}}$ equal to $d_{\text{Na-Cl}}$.

### F. Comments on the use of SIC-LSD

In this subsection we examine more closely some of the approximations to the full SIC-LSD formalism used in this work. We begin with the GSUO approximation, the technique we have used to calculate the transition energies given in Table I. The GSUO technique is physically motivated, rather than formally derived from SIC-LSD total-energy expressions. Its use is based on the identification of the SIC-LSD eigenvalues with electron ionization energies; thus, the GSUO transition energies are represented simply as differences in the relevant eigenvalues. It is appropriate to carefully consider the relationship between GSUO transition-energy results and SIC-LSD total-energy differences. In Ref. 26 a more rigorous scheme for calculating transition energies in SIC-LSD is presented. In this scheme, the exact SIC-LSD total-energy difference between two electronic configurations, differing by the excitation of a single electron from an orbital $a$ to a higher-lying orbital $b$, is cast in the form of an integral over an occupation parameter specifying the relative occupation of the two configurations. The integrand used in this procedure involves the eigenvalues for the active orbitals, $\varepsilon_a$ and $\varepsilon_b$, and a correction term, all readily calculated. This integrand has the important property that it is a nearly linear function of the occupation parameter $\omega$, making the integral (i.e., the transition energy) easy to approximate by evaluating the integrand at a few values of $\omega$. This is demonstrated numerically in Ref. 26 for selected transitions in first- and second-row atoms. The results of one-, two-, and three-point approximation schemes used in that work are in very good agreement with one another, and with the exact SIC-LSD transition energies obtained by total-energy differences. By representing the transition energy as the difference between the eigenvalues of the active orbitals (along with the correction term in the integral method), both the integral technique of Ref. 26 and the GSUO approximation avoid directly calculating $E_t^{\text{SIC-LSD}}(N^*) - E_t^{\text{SIC-LSD}}(N)$ ($N^*$ and $N$ refer to the orbitals of the excited and ground configurations, respectively), which, in the case of large, multiatom systems, requires prohibitive accuracy in determining the respective total energies. The particular utility of the GSUO procedure is that it allows the simple determination of all the excited-state energies from a single SCF calculation. The method of Ref. 26, by contrast, requires at least one distinct SCF calculation for each transition.

As a check on the GSUO results for the NaCl:$Cu^+$ transitions, we used the one-point approximation scheme of Ref. 26 to determine the energy of the $3de_g \rightarrow 4s$ transition. We refer the reader to Ref. 26 for full details concerning this method. In the one-point approximation, the transition energy is

$$E_t^{\text{SIC-LSD}}(N^*) - E_t^{\text{SIC-LSD}}(N) = \varepsilon_{4s} - \varepsilon_{3de_g} + \Delta \ , \tag{26}$$

where

$$\varepsilon_{4s} = \langle \psi_{4s} | H^{\text{LSD}}[N^*] + V_{4s}^{\text{SIC}} | \psi_{4s} \rangle \ , \tag{27}$$

$$\varepsilon_{3de_g} = \langle \psi_{3de_g} | \tilde{H}^{\text{LSD}} + V_{3de}^{\text{SIC}} | \psi_{3de_g} \rangle \ , \tag{28}$$

and

$$\Delta = \left( \frac{6}{\pi} \right)^{1/3} \int d\mathbf{r} \{ \tfrac{3}{4} [\rho(N)^{4/3} - \rho(N^*)^{4/3}] + \tfrac{1}{4} [(\rho_{3de_g})^{4/3} - (\rho_{4s})^{4/3}] + \rho_{4s} \rho(N^*)^{1/3} - \rho_{3de_g} \rho(N)^{1/3} \} \ . \tag{29}$$

In the above equations, $\rho(N^*)$ and $\rho(N)$ are the excited- and ground-configuration spin-up densities, respectively,

and $\rho_i$ is the appropriate orbital density. $H^{\mathrm{LSD}}[N^*]$ is the conventional LSD Hamiltonian corresponding to the excited configuration [see Eq. (6)], whereas $\tilde{H}^{\mathrm{LSD}}$ is a composite of $H^{\mathrm{LSD}}[N^*]$ and $H^{\mathrm{LSD}}[N]$ (see Ref. 26). The orbitals $\psi$ for both the excited and ground configurations used in evaluating these expressions come from a single SCF calculation, based on a composite energy functional consisting of equal parts, $E_t[N^*]$ and $E_t[N]$. We have omitted the spin indices in these equations to avoid unnecessary notation. Since we are considering the spin-preserving transition $3d_\uparrow \rightarrow 4s_\uparrow$, all the spin-dependent quantities above are assumed to carry the $\uparrow$ index.

Using the single-point integral approximation, we calculate a value of 4.10 eV for the $3de_g \rightarrow 4s$ transition energy. This compares well with the GSUO result of 4.77 eV shown in Table I, and demonstrates the reliability of the GSUO approximation for NaCl:$Cu^+$. The agreement seen here is representative of the close correspondence between the GSUO results of Ref. 12 and those obtained using the integral scheme of Ref. 26 for transitions in first-row atoms. Both methods discussed here assume spin-preserving transitions, $\psi_{a\uparrow} \rightarrow \psi_{b\uparrow}$, so that the calculated transition energies correspond to the average of the singlet and triplet transitions. The experimental values in Table I are the singlet-transition energies. If the free-ion singlet-triplet splitting (0.44 eV) is taken as an estimate of the analogous splitting in the impurity crystal, the experimental value corresponding to the spin-preserving transition would be about 4.14 eV, which is intriguingly close to the integral-approximation result. Further analysis of this point would be desirable.

Throughout this work we have distinguished between the local orbitals (LO's), used to generate the SIC potentials $V^{\mathrm{SIC}}$ [Eq. (7)], and the canonical orbitals, which we obtain from the SCF equations [Eq. (10)] and are directly associated with the eigenvalues. In the formal derivation of the SIC-LSD SCF equations, the LO's (and using them, the canonical orbitals) are precisely defined through the SCF equations and a set of auxiliary conditions, the localization equations (LE's) [Eq. (8)]. Formally, the LE's ensure that $E_t^{\mathrm{SIC\text{-}LSD}}$ is extremized by the (exact) LO's. The LE's are, however, very difficult to satisfy exactly for low-symmetry systems such as point defects; treating the LE's requires an additional loop in the SCF process, requiring the generation of SIC potentials for generally complicated LO's, which in multiatom systems have very small but nonzero components on many ion sites. In practice, the LE's may not be necessary in many cases to determine LO's appropriate for use in calculations. While the exact LO's guarantee a lower $E_t^{\mathrm{SIC\text{-}LSD}}$, the improvement over approximate LO's may be quite small. In atomic calculations, the SIC-LSD orbital energies obtained while rigorously satisfying the LE's are only slightly lower than those obtained in calculations neglecting these equations. For atomic lithium, for example, neglecting the LE's results[25] in $1s$ and $2s$ orbital energies of $-2.478$ and $-0.196$ a.u., while the corresponding results obtained by satisfying the LE's are $-2.479$ and $-0.200$ a.u. Furthermore, the canonical orbitals arising from these two calculations for Li are virtually identical, giving a further evidence that the LE's may be reasonably neglected in this case. For multiatom systems, Erwin and Lin,[13] in their calculations of pure alkaline halide band structures, use various approximations to the VB Wannier functions, the exact LO's for those systems. They found that the SIC-LSD band gap was largely insensitive to the approximate LO's used. In our SIC-LSD calculation for NaCl:$Cu^+$, we tested the $3de_g \rightarrow 4s$ transition energy against the form of the $Cu^+$ $3d$ LO's used. Treating the $Cu^+$ $3d$ eigenfunctions, which have definite multicenter character (evidenced by the electron-population results), as the LO's yields the transition energy reported in Table I, 4.77 eV. When the single-center free-ion $Cu^+$ $3d$ orbitals are used for the LO's instead, the calculated transition energy is 4.68 eV, indicating that the precise form of the approximate LO's is not critical in the NaCl:$Cu^+$ calculation.

## IV. CONCLUSIONS

In this work we have described the application of the SIC-LSD theory to the NaCl:$Cu^+$ impurity system. In contrast to earlier local-density calculations for impurity systems, no empirical exchange parameter is used in the present calculation. We obtain results for the fundamental $Cu^+$ $3d \rightarrow 4s$ transitions in good agreement with experiment. For the $3d \rightarrow 4p$ transitions, our calculated energies are about 1 eV higher than the experimental values. This discrepancy may be partly due to the uncertainty in extracting the experimental value of the $3d \rightarrow 4p$ transition energy from the observed broad absorption peak. The embedded-cluster approach used in this calculation explicitly includes host-crystal states out to the seventh-near-neighbor shell around the impurity site, providing a clear picture of the impurity states in NaCl:$Cu^+$. We find well-localized impurity states corresponding to the free-ion $Cu^+$ $3d$ states, and less localized $Cu^+$ $4s$ and $4p$ states. The $4p$ states, in particular, extend well beyond the first-near-neighbor $Cl^-$ shell, making their description by simple impurity-ligand models of the impurity crystal impractical. The character of the various impurity states is used to explain the observed increase in the $3d \rightarrow 4s$, and the decrease in the $3d \rightarrow 4p$, NaCl:$Cu^+$ transition energies compared with the analogous free-ion transitions.

The success of SIC-LSD in predicting the broad features of the impurity absorption spectrum demonstrated in this work suggests investigating refinements to the theory which would permit a detailed look at the fine-structure features of the spectrum. Multiplet splittings and spin-orbit effects have been included in other calculations[19,22] for NaCl:$Cu^+$, giving rise to a useful understanding of the transition and emission processes involving the low-lying excited states. To be generally useful in analyzing impurity spectra, however, quantitative accuracy, of the sort provided by SIC-LSD for the broad spectral features, is required. By obtaining SIC-LSD transition energies through an integral over a fractional occupation parameter,[26] spin-polarized calculations may be performed, making possible the calculation of singlet-triplet splittings of the excited states. The multiplet structure would then provide a starting point for investi-

gating spin-orbit effects. We are developing such an approach for application to NaCl:$Cu^+$-type systems.

It remains a challenge to use SIC-LSD to determine the relaxation of the host-crystal lattice around the impurity site. Previous calculations[19,22] have given conflicting results regarding the Cu-Cl spacing in NaCl:$Cu^+$; physical arguments suggest $d_{Cu\text{-}Cl}$ should be nearly equal to the Na-Cl spacing in NaCl, but cannot be used to obtain a precise value. Because the calculated electronic structure may vary significantly with $d_{Cu\text{-}Cl}$, it is important to determine the equilibrium spacing in order to fully assess the success of SIC-LSD in predicting the impurity transition energies.

Another interesting problem is the electronic structure of KCl:$Cu^+$. This system has a qualitatively different absorption spectrum than either LiCl:$Cu^+$ or NaCl:$Cu^+$.[14,15,20] It is likely that the different appearance of the KCl:$Cu^+$ spectrum is due to the off-center position of $Cu^+$ relative to a $K^+$ site in the KCl lattice;[20] the defect ion sits squarely on a cation site in the other two systems.[19,33] It would be interesting to determine the properties of KCl:$Cu^+$, both for an on-site placement of the impurity ion and for the off-center placement. The properties of the centrosymmetric system would be interesting for comparison with the corresponding properties of LiCl:$Cu^+$ and NaCl:$Cu^+$. In particular, it would be interesting to determine the bonding character of the $Cu^+$ $3d$ states, which, as discussed in Sec. IV D, is expected to differ from that found in other systems. The calculated properties of the off-center system, on the other hand, would be interesting for comparison with experiment.

Finally, the application of the SIC-LSD techniques to other impurity systems, for example, $Ag^+$ impurities, is yet another direction for future work. While the free-ion electronic structures of $Cu^+$ and $Ag^+$ are very similar, the absorption spectra observed for the $Ag^+$ impurities are more complicated[14] than the corresponding $Cu^+$ impurity spectra, comprising more bands. The host-defect bonding in the $Ag^+$ systems occurs between the $Ag^+$ $4d$ and the ligand valence orbitals, and is more pronounced than the $Cu^+$ $3d$ bonding in the $Cu^+$ systems, because of the greater extent of the $4d$ orbitals. It would be interesting to use the SIC-LSD theory to calculate the electronic structure of the $Ag^+$ impurities to explain the absorption spectra differences. Preliminary results[37] for the LiCl:$Ag^+$ system suggest that the complex appearance of the LiCl:$Ag^+$ spectrum is due in part to the large mixing of the $Ag^+$ $4d$ and $Cl^-$ $3p$ orbitals in the impurity eigenstates. As a result of this mixing, several of the impurity states in the VB region have significant admixtures of $Ag^+$ $4d$ orbitals, making transitions from each of these states to the $Ag^+$ $5s$ state possible. Further work on this calculation is currently in progress.

## ACKNOWLEDGMENTS

We are indebted to S. C. Erwin for use of his BAND-AID program package for the NaCl pure-crystal calculation. We also wish to thank Dr. R. A. Heaton and Dr. M. R. Pederson for valuable discussions and programming assistance. Discussions with Dr. D. S. McClure about his experimental works have been especially enlightening. This work was supported by the U. S. National Science Foundation under Grant No. DMR-85-00458.

[1]P. Hohenberg and W. Kohn, Phys. Rev. **136**, B864 (1964).
[2]W. Kohn and L. J. Sham, Phys. Rev. **140**, A1133 (1965).
[3]O. Gunnarsson and B. I. Lundqvist, Phys. Rev. **B13**, 4274 (1976).
[4]J. C. Slater, *The Self-Consistent Field for Molecules and Solids* (McGraw-Hill, New York, 1974).
[5]V. Fock, Z. Phys. **61**, 126 (1930); J. C. Slater, Phys. Rev. **35**, 210 (1930); D. R. Hartree, Proc. Cambridge Philos. Soc. **24**, 426 (1928).
[6]J. P. Perdew and A. Zunger, Phys. Rev. B **23**, 5048 (1981).
[7]R. A. Heaton and C. C. Lin, J. Phys. C **17**, 1853 (1984).
[8]T. Koopmans, Physica **1**, 104 (1934).
[9]K. Schwarz, Phys. Rev. B **5**, 2466 (1972).
[10]J. G. Harrison and C. C. Lin, Phys. Rev. B **23**, 3894 (1981).
[11]I. Lindgren, Int. J. Quantum Chem. Symp. **5**, 411 (1971).
[12]J. G. Harrison, R. A. Heaton, and C. C. Lin, J. Phys. B **16**, 2079 (1983).
[13]S. C. Erwin and C. C. Lin, J. Phys. C **21**, 4285 (1988).
[14]K. Fussgänger, W. Martienssen, and H. Bilz, Phys. Status Solidi **12**, 383 (1965).
[15]K. Fussgänger, Phys. Status Solidi **34**, 157 (1969); **36**, 645 (1969).
[16]R. S. Knox, J. Phys. Soc. Jpn., Suppl. II **18**, 268 (1963).
[17]K. L. Yip and W. B. Fowler, Phys. Status Solidi B **53**, 137 (1972).
[18]C. Pedrini, A. Chermette, A. B. Goldberg, D. S. McClure, and B. Moire, Phys. Status Solidi B **120**, 753 (1983); B. Moire, H. Chermette, and C. Pedrini, J. Chem. Phys. **85**, 2784 (1986).
[19]H. Chermette and C. Pedrini, J. Chem. Phys. **77**, 2460 (1982); **75**, 1869 (1981).
[20]S. A. Payne, A. B. Goldberg, and D. S. McClure, J. Chem. Phys. **81**, 1529 (1984).
[21]N. W. Winter, R. M. Pitzer, and D. K. Temple, J. Chem. Phys. **86**, 3549 (1987).
[22]N. W. Winter, R. M. Pitzer, and D. K. Temple, J. Chem. Phys. **87**, 2945 (1987).
[23]R. A. Heaton, J. G. Harrison, and C. C. Lin, Phys. Rev. B **31**, 1077 (1985).
[24]M. R. Pederson, R. A. Heaton, and C. C. Lin, J. Chem. Phys. **80**, 1972 (1984).
[25]M. R. Pederson, R. A. Heaton, and C. C. Lin, J. Chem. Phys. **82**, 2688 (1985).
[26]R. A. Heaton, M. R. Pederson, and C. C. Lin, J. Chem. Phys. **86**, 258 (1987).
[27]S. Nakai and T. Sagawa, J. Phys. Soc. Jpn. **26**, 1427 (1969).
[28]J. G. Harrison, J. Chem. Phys. **78**, 4562 (1983).
[29]C. E. Morre, *Atomic Energy Levels,* Natl. Bur. Stand. (U.S.) Circ. No. 467 (U.S. GPO, Washington, D.C., 1952), Vol. 2.
[30]W. Kohn and J. R. Onffroy, Phys. Rev. B **8**, 2485 (1973).
[31]W. P. Menzel, K. Mednick, C. C. Lin, and C. F. Dorman, J. Chem. Phys. **63**, 4708 (1975).
[32]R. L. Chien, J. Simonetti, and D. S. McClure, J. Lumin. **31-32**,

326 (1984).
[33]J. Simonetti and D. S. McClure, Phys. Rev. B **16**, 3887 (1977).
[34]R. S. Mulliken, J. Chem. Phys. **23**, 1833 (1955); **23**, 1841 (1955).
[35]T. Ziegler, A. Rauk, and E. J. Baerends, Theor. Chim. Acta **43**, 261 (1977).
[36]S. Y. Shashkin and W. A. Goddard III, Phys. Rev. B **33**, 1353 (1986).
[37]K. A. Jackson and C. C. Lin (unpublished).